

THERMAL INSTABILITY INDUCED INTERSTELLAR TURBULENCE

ALEXEI KRITSUK¹ AND MICHAEL L. NORMAN

Physics Department and CASS, University of California, San Diego, CA 92093-0424

akritsuk@ucsd.edu, mnorman@cosmos.ucsd.edu

Submitted to *ApJ Letters*, December 29, 2018

ABSTRACT

We study the dynamics of phase transitions in the interstellar medium (ISM) by means of three-dimensional hydrodynamic numerical simulations. We use a realistic cooling function and generic nonequilibrium initial conditions to follow the formation history of a multi-phase medium in detail in the absence of gravity. We outline a number of qualitatively distinct stages of this process, including a linear isobaric evolution, transition to an isochoric regime, formation of filaments and voids (also known as ‘thermal pancakes’), the development and decay of supersonic turbulence, approach to pressure equilibrium, and final relaxation of the multi-phase medium. We refer to previous analytical studies for a number of nonlinear effects of thermal instability in order to identify them in our numerical models. We discuss the role of initial conditions, radiative cooling and heating, and build up a comprehensive scenario for the development of phase transitions in the ISM. While not all initial conditions yield a stable two-phase medium, we examine such a case in detail. We find that the two phases are well mixed with the cold clouds possessing a fine-grained structure near our numerical resolution limit. We find that the amount of gas in the intermediate unstable phase roughly tracks the rms turbulent Mach number, peaking at 25% when $M_{rms} \sim 8$, decreasing to 11% when $M_{rms} \sim 0.4$.

Subject headings: hydrodynamics — instabilities — ISM: structure — turbulence

1. INTRODUCTION

Thermal instability (TI) has many implications in astrophysics (clumpy interstellar medium (ISM), stellar atmospheres, star formation, globular cluster and galaxy formation, etc.) as well as in laboratory plasma physics (‘over-heating’ instability, ‘marfes’ in tokamaks, etc.), see Meerson (1996) for a recent review. The instability may be driven by radiative cooling of optically thin gas (a variant known as ‘radiation-driven TI’) or by exothermic nuclear reactions (so-called Schwarzschild & Härm (1965) instability causing helium-shell flashes in Population II stars).

Linear stability theory for a medium with volumetric sources and sinks of energy in thermal equilibrium was developed by Field (1965), who identified three unstable modes: (i) *isobaric* mode (pressure driven formation of condensations not involving gravitation and (ii) two *isentropic* modes (overstability of acoustic waves propagating in opposite directions). Hunter (1970, 1971) extended these results to an arbitrary nonstationary background flow, showing that cooling-dominated media are potentially more unstable than those in equilibrium, while heating provides stabilization.

The most common applications of thermal instability to the ISM and star formation deal with the isobaric mode which was employed to explain the observed multi-phase structure of the ISM (Pikel’ner 1968; Field, Goldsmith, & Habing 1969; McKee & Ostriker 1977; McKee 1990; Wolfire et al. 1995). This particular form of TI is also known as ‘radiative-condensation instability’ (Aranzon, Meerson, & Sasorov 1993).

Analysis of infinitesimal perturbations gives two characteristic length-scales for the isobaric condensation mode: (i) a cooling scale $\lambda_p = c/\omega_p$ (where c is the adiabatic

sound speed and ω_p is the growth rate); (ii) a critical scale $\lambda_\kappa = c\sqrt{t_d/\omega_p}$ (where t_d is the characteristic thermal diffusion time). These two length-scales define short-, intermediate-, and long-wavelength limits (Meerson 1996; Kovalenko & Shchekinov 1978). In the short-wavelength limit small isobaric perturbations are inhibited by heat conduction, so that $\omega_p < 0$ for $\lambda < \lambda_\kappa$. In the long-wavelength limit the perturbations cannot grow isobarically due to finite sound speed effects and thus $\omega_p \rightarrow 0$ for $\lambda/\lambda_p \rightarrow \infty$. This is only true if the gas is *isochorically* stable (Parker 1953; Field 1965; Shchekinov 1978), otherwise the growth rate remains finite: $\omega_p \rightarrow \omega_p > 0$ for $\lambda/\lambda_p \rightarrow \infty$, but only large-scale temperature perturbations are growing, thus resulting in pressure variations and the formation of shock waves. The growth rates and characteristic scales depend on the heating and cooling properties of a given medium. Under the ISM conditions, if one assumes thermal equilibrium (i.e. exact balance between cooling and heating), isochoric instability manifests itself only at relatively high temperatures, $T \gtrsim 10^5$ K. However, in cooling dominated regimes it can develop at temperatures as low as 10^3 K.

A specific feature of TI in the ISM is a large ($\gtrsim 1$ dex) gap in gas densities between the two stable phases. The density range of interest in a galaxy formation context is even larger. This implies the importance of nonlinear effects in the dynamics of phase transitions. Nonlinearity brings into play nonequilibrium effects. Already weakly nonlinear development of condensations in an initially homogeneous gas in thermal equilibrium drives the system away from equilibrium. The mean pressure drops since $\bar{\rho}^2 > \bar{\rho}^2$ and cooling overcomes heating globally (Kritsuk 1985). Later, on a time-scale of $\sim \omega_p^{-1}$, as condensa-

¹ Also Sobolev Astronomical Institute, St. Petersburg State University, Russia.

tions get denser and cooler, the isobaric condition $\lambda \ll \lambda_p$ becomes violated locally within them, so the system departs from pressure equilibrium. These effects are essential for the isobaric mode of TI in the ISM and star formation contexts. Therefore, analytical nonlinear solutions to ‘isobarically’-reduced TI-equations are insufficient to describe the radiative stage of the phase transition ($t \sim \frac{1}{\omega_p}$).

During this strongly nonlinear stage *large-scale* condensations form in such a way that gas moves almost inertially and its kinetic energy dominates thermal energy ($p \ll \rho v^2$). Accordingly, the gas velocities in these condensations are of the order of the sound speed in the unperturbed state. The situation here is directly analogous to the long-wave gravitational instability, so that results concerning the origin of cellular structure and Zel’dovich (1970) ‘pancakes’ can be entirely carried over to the case of long-wave thermal instability (Meerson & Sasorov 1987). Sasorov (1988) gave an elegant proof to qualitatively the same result as applies to *small-scale* thermal instabilities, i.e. the onset of TI produces voids and highly flattened condensations along certain two-dimensional surfaces. These are also called Sasorov’s or ‘thermal’ pancakes (Meerson 1996). The formation of filaments was simultaneously noticed in two-dimensional numerical simulations of TI in the solar transition region (Dahlburg et al. 1987; Karpen, Picone & Dahlburg 1988). Ever since thermal pancakes are being rediscovered both analytically and in numerical simulations (e.g., Lynden-Bell & Tout (2001)).

Thermal pancakes are transient. However, what happens next, before the evolution turns to a conductive relaxation stage (Meerson 1996), until recently has remained the ‘terra incognita’ of TI-theory. The problem of ‘post-radiative’ mechanical relaxation toward a static multi-phase medium requires a solution for the full set of hydrodynamic equations which can only be obtained numerically. One-dimensional simulations pioneered by Goldsmith (1970) demonstrated that TI develops large motions in the ISM (see also Hennebelle & Péault (1999) for an example of how large motions can trigger TI). For some time progress in this direction was precluded by numerical difficulties in modeling convergent cooling flows with high Mach numbers and high density contrasts (e.g., Vázquez-Semadeni, Gazol, & Scalo (2000)). Recent multi-dimensional numerical simulations of the ISM evolution in disk-like galaxies include effects of gravity, star formation and supernova feedback (Wada & Norman 2001; Wada 2001). However, it is hard to determine the role of TI in shaping the ISM structures found in these models, partly because the simulations still do not resolve length-scales important for TI and partly due to the additional physical effects.

A study of long-term evolution of a bistable medium with a conductive interface between the phases (Zel’dovich & Pikel’ner 1968) showed that thermal waves (interfaces) propagate to establish a unique equilibrium pressure in a *static* two-phase medium. The pressure value is determined by the ‘area rule’ and depends only on the heating and cooling functions. This line of research was later developed both analytically and numerically by Doroshkevich & Zeldovich (1981); Elphick, Regev, & Spiegel (1991); El-

phick, Regev, & Shaviv (1992); Aranson et al. (1993); Aranson, Regev, & Shaviv (1994); Shaviv & Regev (1994) and others. On a much longer time-scale conductive relaxation is followed by the weak interaction of conductive fronts which accelerates them and causes front annihilation upon collisions (Dimitis & Meerson 1991; Meerson 1996). These results, based on solutions to a reaction-diffusion equation, remain mostly of academic interest for ISM conditions until the missing link between thermal pancakes and static multi-phase medium is established.

The purpose of this Letter is to report on results of three-dimensional numerical simulations of classical TI which fill the gap in theory exploring in detail the late radiative stage and post-radiative relaxation toward a multi-phase medium. Our major result is that formation of thermal pancakes induces turbulence in the ISM which serves as a nonlinear saturation mechanism for TI. As a consequence of a turbulent cascade: (i) information about initial perturbations is lost, including the imprints of heat conduction in the density power spectrum during the the linear stage; (ii) turbulent diffusion becomes the dominant transport mechanism during the post-radiative relaxation stage.

2. SIMULATIONS

We solve the equations of ideal gas dynamics (Eqs. (6)-(9) in Field (1965)) in a cubic domain with periodic boundary conditions, assuming zero conductivity and no gravity. The generalized cooling function \mathcal{L} contains cooling and heating terms, $\mathcal{L} = \rho\Lambda(T, Z) - \Gamma$. The temperature dependence of radiative cooling $\Lambda(T, Z)$ for $T \in [10, 10^8]$ K is taken from Spaans (2000); Wada & Norman (2001). The gas metallicity Z is assumed to be solar in most of the models, but we also considered a case with a subsolar value of $0.1Z_\odot$. For simplicity we assume that the heating rate $\Gamma \equiv \text{const}$, and we define it in units of the cooling rate in an initial unperturbed state: $\Gamma = Q\rho_0\Lambda(T_0, Z)$, where $Q \in \{0, 0.01, 0.1, 0.5, 1\}$. The initial unperturbed state is uniform with gas density $\rho_0 \in \{1.67 \times 10^{-25}, 1.67 \times 10^{-24}\}$ g cm⁻³ and gas temperature $T_0 \in \{7000, 2 \times 10^6\}$ K. The box size $L \in \{5, 100, 500\}$ pc was chosen such that at least the cooling scale $\lambda_{p,0}$ for initial state is well resolved on a discrete grid of 128^3 or 256^3 cells. In most cases we impose initial perturbations as an isobaric noise with a power spectrum index -3 , *rms* deviation of $\varepsilon = 0.05$, and high-wavenumber cutoff $k_{max} \in \{8, 32\}$ ², assuming zero initial velocities. A few cases were started up with random velocity perturbations, varying the amplitude, and assuming uniform initial density.

The simulations were performed using two hydrosolvers implemented in the Enzo code developed by Bryan & Norman (1999): one is a direct Eulerian version of the PPM-scheme (Colella & Woodward 1984), and the other is the finite difference Eulerian method originally implemented in ZEUS (Stone & Norman 1992).

3. RESULTS

Here we present results for our fiducial model computed on a ‘moderate’ resolution grid of 256^3 cells assuming

² These are normalized values, $k_{max} = 32$ for a grid 256^3 implies that the cutoff-scale spans 8 grid-zones. This is slightly below the dissipation limit of our numerical scheme.

$L = 5$ pc, $\rho_0 = 1.67 \times 10^{-24}$ g cm $^{-3}$, $T_0 = 2 \times 10^6$ K, $Q = 0.1$, solar metallicity, and isobaric perturbations with $\varepsilon = 0.05$, $k_{max} = 32$. With these initial conditions the linear isobaric mode develops on a time-scale $\omega_{p,0}^{-1} \approx 0.3$ Myr, the cooling length $\lambda_{p,0} \approx 70$ pc, and the critical length for heat conduction $\lambda_{\kappa,0} \approx 8$ pc. Thus, our initial perturbations formally drop into a short-wavelength limit.³ Assumed cooling and heating rates and the value of initial gas density imply the existence of attracting bistable thermal equilibrium with physical conditions close to those in the ISM (Fig. 2), although the pressure range for bistability is somewhat narrower than in a ‘standard’ model of Wolfire et al. (1995).

With our setup heating does not compensate cooling in the initial state, thus TI sets in on a time-dependent background state. As the gas cools, the instability channels a part of its internal energy into kinetic energy of converging flows which create condensations and evacuate gas from under-dense voids (Fig.3). Growing density variance accelerates cooling efficiency, so the gas as a whole cools much faster than a homogeneous medium with the same initial setup. Since initial perturbations span a range of linear scales, the epoch of thermal pancakes’ formation lasts from ~ 0.07 , when the first cold blob forms, till ~ 0.1 Myr, when the mean kinetic energy and then pressure variance reach their maximal values (see Figs 1a,b, 2a, and 3).

The pancakes themselves exhibit a rather complex inner structure. As the isobaric compression gives way to isochoric cooling (Kritsuk 1990; Burkert & Lin 2000), accretion shocks develop within the cooling condensations at temperatures corresponding to two strips of stability in the phase pane (Fig. 2a). Dense gas in the cores of condensations cools further as it contracts in a regime similar to explosive condensation described in Meerson & Sasorov (1987), see Fig. 2a.

Due to asymmetries in the initial conditions the dense cores gain nonzero momentum which drives a bottom-up collapse of the hierarchical cellular structure composed of thermal pancakes. As a result a single large void forms in the periodic box and ρ_{min} attains its global minimum by $t = 0.13$ Myr. (Figs 1c and 3). At this point the gas density variance approaches its maximum and the density spans a range of 5.5 dex. The highest density gas quickly relaxes to thermal equilibrium, however, the dense cold blobs reexpand slightly until they reestablish pressure balance with the less dense environment, so the mass fraction of the gas in cold stable phase ‘H’⁴ decreases, see Fig. 3.

By $t \approx 0.15$ Myr the information about details of initial perturbations is lost and highly compressible supersonic turbulence with rms Mach number of about 10 is fully developed in the computational domain (Fig. 3). The velocity power spectrum attains its ‘universal’ shape, which then only slightly evolves on a time scale of ~ 1 Myr as turbulence decays ($\langle E_k \rangle \approx 5.4 \times 10^{11} (t/0.3 \text{ Myr})^{-2}$ erg cm $^{-3}$ for $t \in (0.3, 1.7)$ Myr, cf. Mac Low, Klessen, & Burkert (1998)). The density probability distribution function (PDF) exhibits a power-law

³ Since initial perturbations are not infinitesimal, $\frac{\delta\rho}{\rho}|_{max,0} = 0.23$, TI reaches strongly nonlinear regime by 0.07 Myr. For such perturbations both $\lambda_{p,0}$ and $\lambda_{\kappa,0}$ are effectively lower than their linear estimates.

⁴ We follow the notation of Field et al. (1969).

⁵ For $\Lambda(T) \propto T^\alpha$ and $\Gamma = const$ equilibrium pressure $p_{eq} \propto \rho_{eq}^{1-\frac{1}{\alpha}}$ and, since $\alpha > 1$ at low temperatures, the effective adiabatic index $\gamma_{eq} < 1$.

⁶ It was the necessity to resolve isobaric mode in the vicinity of bistable thermal equilibrium that forced us to choose the box size $L = 5$ pc.

excess at high densities, where the ‘effective’ equation of state is soft⁵ (cf. Passot & Vázquez-Semadeni (1998)). Low density gas is nearly adiabatic, $\gamma = \frac{5}{3}$, therefore the PDF also has a power-law regime at low ρ (Fig. 2c,e).

Relaxation time-scales towards thermal and dynamical equilibrium depend on local physical conditions. Cold dense gas quickly settles to a thermal equilibrium, but its dynamical relaxation proceeds quite slowly (by $t = 1.5$ Myr its kinetic energy dominates thermal by up to a factor of 3 in the most dense blobs). Warm tenuous gas, instead, undergoes a fast transition to a subsonic regime with a quite uniform density distribution, see PDFs in Fig. 2e,f, but it takes longer to establish thermal equilibrium. As soon as the system relaxes to a bistable state with pressure close to the allowed minimum, the density PDF shows a bimodal distribution and phase fractions by mass saturate at $\sim 42\%$ for the warm phase, $\sim 44\%$ cold phase, and $\sim 14\%$ of the mass fall in the unstable temperature regime. The substantial amount of gas in the unstable regime can be explained as due to turbulent diffusion. Vorticity is generated by baroclinic instabilities and in shocks, which develop during the radiative stage at the interface of growing condensations (Dahlburg et al. 1987; Karpen et al. 1988). Since at least some part of the gas does not stay in thermal equilibrium (Fig. 2f), the exact fraction of thermally unstable gas should be determined by Hunter’s (1970) TI criterion. A rough estimate, however, could be obtained using density/temperature limits for stability of thermal equilibrium, which are used in Figs 1/3. Note, that such estimates are robust only for a medium in a quasi-isobaric state. One has to be cautious obtaining temperature estimates for the unstable gas based upon assumption of thermal equilibrium (cf. Heiles 2001).

Only since we are able to resolve the length-scales smaller than the cooling scale λ_p in the vicinity of the bistable regime, the gas in the box relaxes to an isobaric state⁶. Seed perturbations in the corresponding range of linear scales are always available to feed the instability provided the turbulent cascade exists. The resulting two-phase medium is dynamic. Turbulent velocities do not correlate with density, and dense clouds appear to be shapeless random aggregations of cold Lagrangian gas parcels, forming a ‘fractal’ substrate (Fig. 1f).

4. DISCUSSION

Our fiducial case was constructed to produce a stable two-phase medium because of its relevance to the Galactic ISM. We are interested in TI over a wide range of conditions as might be found in the ISM of high redshift protogalaxies. We have simulated other cases with different parameter choices which do not produce stable two-phase media. However, we find they all develop turbulence in the nonlinear radiative stage of TI. Here we briefly discuss how the turbulence and asymptotic phase structure depend on initial conditions, deferring a more complete discussion to a future paper. The rms Mach number is a function of the peak mean kinetic energy generated which

in turn depends on the initial temperature. In our fiducial run $\langle E_k \rangle_{max}$ is about 2% of the initial thermal energy (Fig. 3). This fraction is lower, when Q is close to unity, since more gas remains in the hot phase and less kinetic energy is generated by isochoric cooling effects. We also quite naturally obtained lower values of $\mathcal{M}_{rms} \sim 0.3$ in models with equilibrium initial conditions $T_0 = 7000$ K and $Q = 1$. But we would expect higher Mach numbers if the bistable range of pressure were wider than provided by our adopted cooling function. Both equilibrium and non-equilibrium ISM initial conditions produce turbulence via nonlinear TI, since nonlinearity drives the system out of equilibrium.

The initial gas density determines the number and mass fractions of thermal phases in the *relaxed* state depending upon its position relative to the valleys and hills on the thermal equilibrium curve. This is consequence of our choice of constant volume boundary conditions, which means that the mean density in the box remains constant. After the rapid cooling stage our models with low initial densities, $\rho_0 = 1.5 \times 10^{-25}$ g cm⁻³, high temperature $T_0 = 2 \times 10^6$ K, and $Q \in \{0.5, 1\}$ generate turbulence, evolve through a transient three-phase stage, and then relax to a single-phase low-pressure warm ISM. While turbulence is a generic feature of nonlinear saturation of TI, our simulations show that *detailed* turbulent properties and nature of emerging multi-phase medium do depend sensitively on the Mach number and effective equation of state controlled by heating and cooling; this will be discussed elsewhere. Two identical simulations, except that cutoffs in initial power spectra were different ($k_{max} = 8$ and 32 on a 128³ grid, $L = 100$ pc, $Q = 0$), demonstrated considerable structural differences in density distributions at the thermal pancake stage, t_{tp} , and surprisingly similar

'chaotic' density structures and identical velocity power spectra at $\sim 6 t_{tp}$, when turbulent mixing covered the whole computational domain. This implies that the imprints of heat conduction in the density power spectrum during the the linear stage could be erased later by the developing turbulent cascade.

TI is certainly not the only potential source of turbulence in the ISM, but it cannot be ignored at least in those scenarios which actively employ TI to explain the origin and properties of observed objects. We suggest a paradigm shift concerning the role of thermal instability in the ISM and the nature of multi-phase ISM. The idea of 'static' two-phase ISM appreciated since late 60s (pressure confined thermally stable dense clouds embedded in rarefied intercloud gas forming as a result of TI and subject to phase exchange due to cloud evaporation/condensation) must give way to the notion of dynamic multi-phase ISM, in which TI induces slowly decaying turbulence and turbulent diffusion regulates phase exchange processes. In this new emerging picture the dense clouds are shapeless random aggregations of cold Lagrangian gas parcels, the clouds do not preserve their identity in real space on their sound-crossing time-scale until self gravity tightens the fragments up into a self-gravitating cloud to form stars. Our results may suggests modifications to the scenario of three-phase ISM (McKee & Ostriker 1977; McKee 1990; Heiles 2001b) in ways which are yet to be understood.

We are grateful to Marco Spaans for providing cooling functions prior to publication. We acknowledge useful conversations with George Field and Chris McKee. This work was partially supported by NRAC computer grant PQK and utilized the NCSA Silicon Graphics Origin2000 system at the University of Illinois at Urbana-Champaign.

REFERENCES

Aharonson, V., Regev, O., & Shaviv, N. 1994, ApJ, 426, 621
 Aranson, I., Meerson, B., & Sasorov, P. V. 1993, Phys. Rev. E, 47, 4337
 Bryan, G. L., & Norman, M. L. 1999, in IMA Vol. 117, Structured Adaptive Mesh Refinement (SAMR) Grid Methods, ed. S. B. Baden, N. P. Chrisochoides, D. Gannon, & M. L. Norman (New York: Springer), 165
 Burkert, A., & Lin, D. N. C. 2000, ApJ, 537, 270
 Colella, P., & Woodward, P. R. 1984, J. Comp. Phys., 54, 174
 Dahlburg, R. B., Devore, C. R., Picone, J. M., Mariska, J. T., & Karpen, J. T. 1987, ApJ, 315, 385
 Dimitis, A. M., & Meerson, B. 1991, Phys. Fluids B, 3, 1420
 Doroshkevich, A. G., & Zeldovich, I. B. 1981, Zh. Eksp. Teor. Fiz., 80, 801 [Sov. Phys. JETP 53, 405, 1981]
 Elphick, C., Regev, O., & Spiegel, E. A. 1991, MNRAS, 250, 617
 Elphick, C., Regev, O., & Shaviv, N. 1992, ApJ, 392, 106
 Field, G. B. 1965, ApJ, 142, 531
 Field, G. B., Goldsmith, D. W., & Habing, H. J. 1969, ApJ, 155, L149
 Goldsmith, D. W. 1970, ApJ, 161, 41
 Heiles, C. 2001a, ApJ, 551, L105
 Heiles, C. 2001b, ASP Conf. Ser. 231: Tetons 4: Galactic Structure, Stars and the Interstellar Medium, 294
 Hennebelle, P., & Pérault, M. 1999, A&A, 351, 309
 Hunter, J. H., Jr. 1970, ApJ, 161, 451
 Hunter, J. H. 1971, ApJ, 166, 453
 Karpen, J. T., Picone, M., & Dahlburg, R. B. 1988, ApJ, 324, 590
 Kovalenko, I. G., & Shchekinov, Yu. A. 1999, Phys. Plasmas, 6, 335
 Kritsuk, A. G. 1985, Sov. Astron., 29, 39
 Kritsuk, A. G. 1990, Sov. Astron., 34, 21
 Lynden-Bell, D., & Tout, C. A. 2001, ApJ, 558, 1
 Mac Low, M.-M., Klessen, R. S., & Burkert, A. 1998, Phys. Rev. Lett., 80, 2754
 McKee, C. F. 1990, ASP Conf. Ser. 12: The Evolution of the Interstellar Medium, 3
 McKee, C. F., & Ostriker, J. P. 1977, ApJ, 218, 148
 Meerson, V. I., & Sasorov, P. V. 1987, Sov. Phys. JETP, 65, 300
 Meerson, V. I. 1996, Rev. Mod. Phys., 68, 215
 Parker, E. N. 1953, ApJ, 117, 431
 Passot, T., & Vázquez-Semadeni, E. 1998, Phys. Rev. E, 58, 4501
 Pikel'ner, S. B. 1968, Sov. Astron., 11, 737
 Sasorov, P. V. 1988, Sov. Astron. Lett., 14, 129
 Shaviv, N. J., & Regev, O. 1994, Phys. Rev. E, 50, 2048
 Schwarzschild, M., & Härn, R. 1965, ApJ, 142, 855
 Shchekinov, Yu. A. 1978, AZh, 55, 311
 Spaans, M. 2000, Private communication
 Stone, J. M., & Norman, M. L. 1992, ApJS, 80, 753
 Vázquez-Semadeni, E., Gazol, A., & Scalo, J. 2000, ApJ, 540, 271
 Wada, K. 2001, astro-ph/0108339
 Wada, K., & Norman, C. A. 2001, ApJ, 547, 172
 Wolfire, M. G., Hollenbach, D., McKee, C. F., Tielens, A. G. G. M., & Bakes, E. L. O. 1995, ApJ, 443, 152
 Zel'dovich, Ya. B., & Pikel'ner, S. B. 1968, Sov. Phys. JETP, 29, 170
 Zel'dovich, Ya. B. 1970, Astrofizika, 6, 319

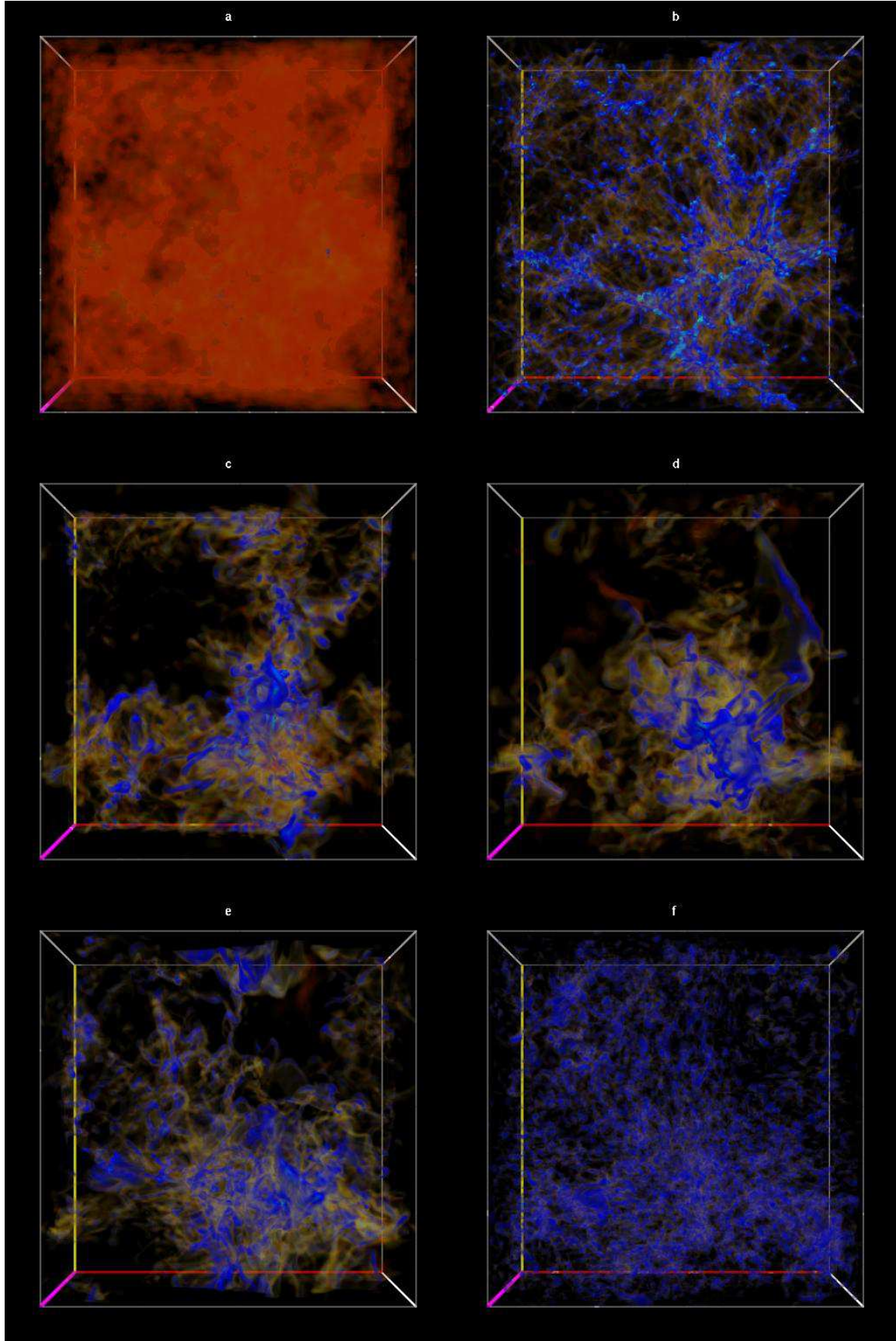


FIG. 1.— Snapshots of the gas density field (perspective volume rendering) (a) the first condensation at $t = 0.07$ Myr; (b) thermal pancakes at $t = 0.1$ Myr; (c) collapse and turbulization of cellular structure at $t = 0.17$ Myr; (d) & (e) turbulent relaxation at $t = 0.3$ and 0.5 Myr; (f) two-phase medium at $t = 1.5$ Myr. 256^3 grid points. Log density color coding: light blue - dense blobs at the intersections of the filaments, $\rho > 10^{-22} \text{ g cm}^{-3}$; blue - stable cold phase, $\rho \in [10^{-23}, 10^{-22}] \text{ g cm}^{-3}$; yellow-to-brown - unstable density regime, $\rho \in [10^{-23.7}, 10^{-23.0}] \text{ g cm}^{-3}$; transparent-red - low density gas, including stable warm phase, $\rho < 10^{-23.7} \text{ g cm}^{-3}$. [See mpeg animations at <http://akpc.ucsd.edu/ThermalLetter/thermal.html>]

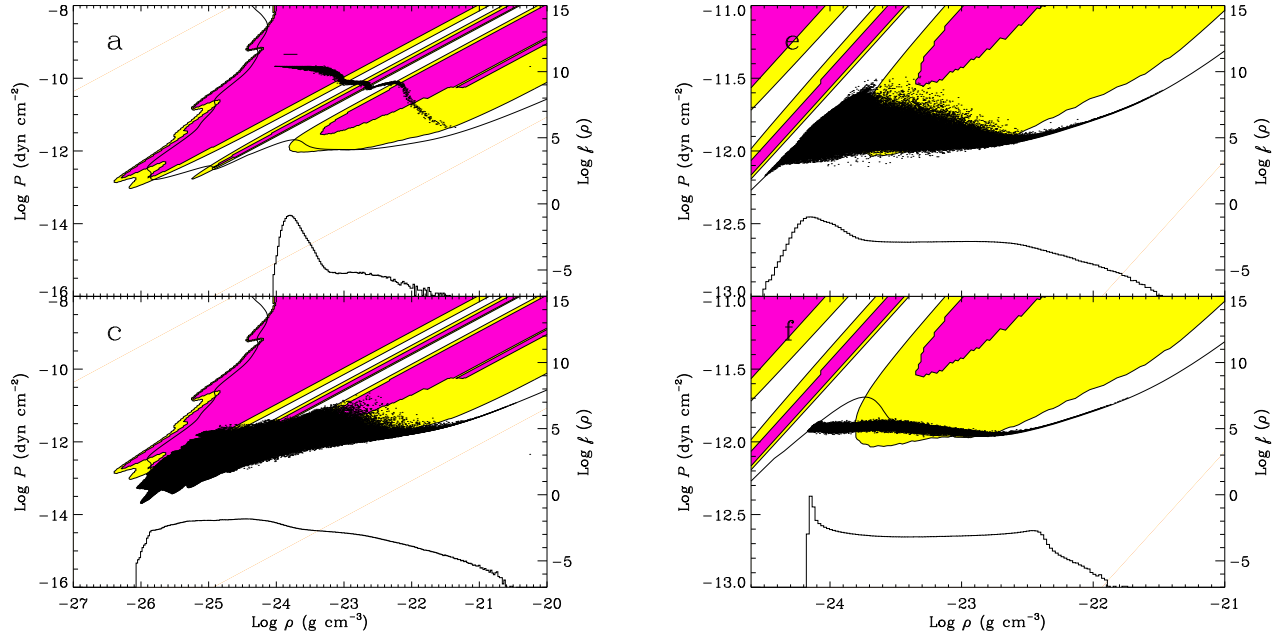


FIG. 2.— Snapshots of phase diagrams (timing and labels correspond to those in Fig. 1): (a) $t = 0.07$ Myr; (c) $t = 0.17$ Myr; (e) $t = 0.5$ Myr; (f) $t = 1.5$ Myr. Black dots show scatter plots of pressure vs. density. The dash at $P = 4.55 \times 10^{-10}$ dyn cm $^{-2}$ in panel (a) shows the initial conditions. Background yellow-filled contours specify the part of the phase plane where isobaric mode is unstable; overlaid magenta contours are the regions of isochoric instability. Heavy solid line shows thermal equilibrium curve. Density PDFs are plotted at the bottom of each panel, see scale to the right.

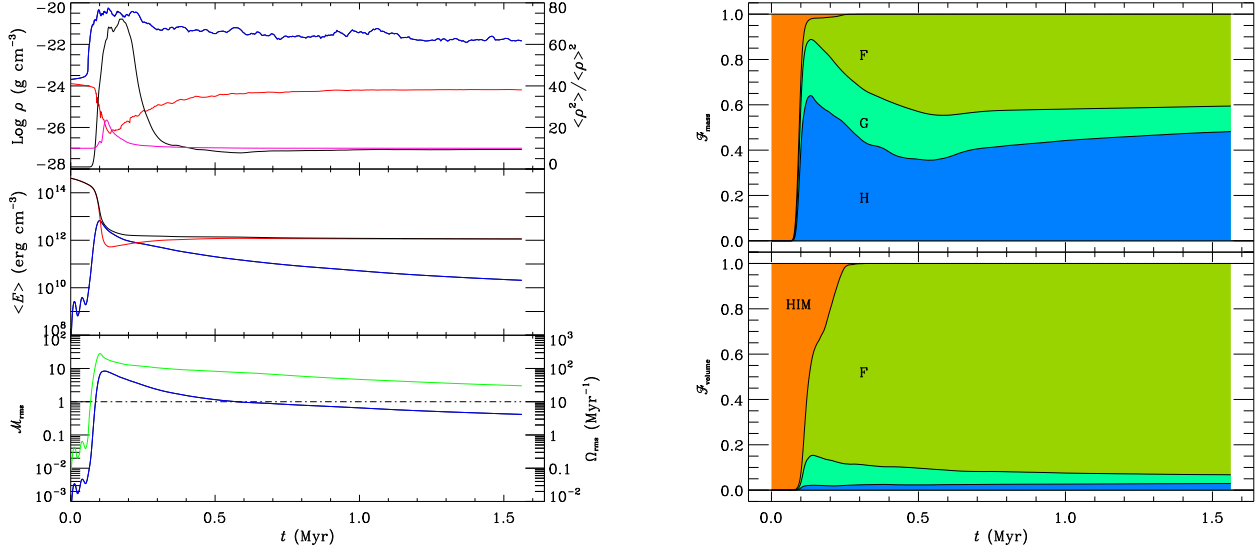


FIG. 3.— Time evolution of global variables. Upper left panel: ρ_{max} (blue), ρ_{min} (red), $\langle \rho^2 \rangle / \langle \rho \rangle^2$ (black), $10 \langle p^2 \rangle / \langle p \rangle^2$ (magenta, scale is at the right). Left in the middle: total energy (black), internal energy (red), kinetic energy (blue). Left lower panel: enstrophy (green), mass weighted rms Mach number (blue). Upper right panel: mass fractions of different thermal phases: hot (label ‘HIM’, $T > 19\,000$ K) warm stable (label ‘F’, $T \in [8\,000, 19\,000]$ K), intermediate unstable (label ‘G’, $T \in [600, 8\,000]$ K), and cold stable (label ‘H’, $T < 600$ K). Lower right panel: the same as above, but for volume fractions.